ACS chemical biology

pubs.acs.org/acschemicalbiology

Articles

Bifunctional Peptide that Anneals to Damaged Collagen and Clusters TGF-β Receptors Enhances Wound Healing

Sayani Chattopadhyay, Leandro B. C. Teixeira, Laura L. Kiessling, Jonathan F. McAnulty, and Ronald T. Raines*

Cite This: *ACS Chem. Biol.* 2022, 17, 314–321

Read Online

ACCESS | Metrics & More | Article Recommendations

ABSTRACT: Transforming growth factor-β (TGF-β) plays important roles in wound healing. The activity of TGF-β is initiated upon the binding of the growth factor to the extracellular domains of its receptors. We sought to facilitate the activation by clustering these extracellular domains. To do so, we used a known peptide that binds to TGF-β receptors without diminishing their affinity for TGF-β. We conjugated this peptide to a collagen-mimetic peptide that can anneal to the damaged collagen in a wound bed. We find that the conjugate enhances collagen deposition and wound closure in mice in a manner consistent with the clustering of TGF-β receptors. This strategy provides a means to upregulate the TGF-β signaling pathway without adding exogenous TGF-β and could inspire means to treat severe wounds.

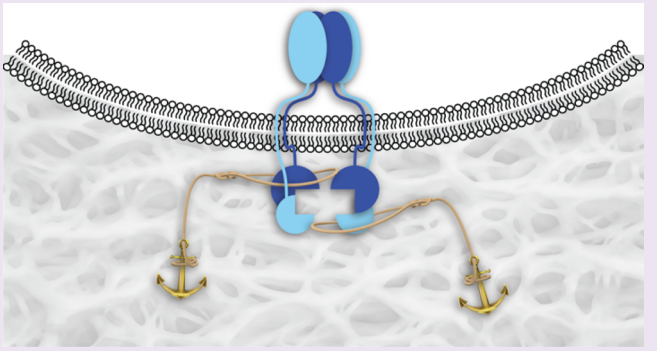

INTRODUCTION

The transforming growth factor β (TGF-β) family is a group of mammalian secretory proteins that play myriad roles in development and disease.[1−4] Their biological activities are initiated upon interaction with two type-I receptors (TβRI) and two type-II receptors (TβRII).[5−7] These cell−surface receptors are characterized by an extracellular TGF-β-binding domain, a transmembrane domain, and a cytosolic serine/threonine kinase domain.[8] Upon binding to TGF-β, TβRII recruits TβRI into an activated heterotetrameric complex (Figure 1A). The cytosolic domain of TβRII then catalyzes the phosphorylation of the regulatory region of TβRI and thereby activates the adjacent serine/threonine kinase domain, ultimately leading to the phosphorylation of downstream effectors, Smad2 and Smad3, which translocate to the nucleus and mediate the gene expression.

Activation of the TGF-β signaling cascade can promote dermal fibrosis.[9−13] For example, TGF-β administered to full-thickness wounds in rabbits by encapsulation in a collagen-sponge scaffold accelerates re-epithelialization and contraction.[14] Similarly, TGF-β applied topically or by injection heals wounds by increasing the tensile strength and promoting fibroblast proliferation and collagen deposition.[15−20] These approaches, however, require the administration of exogenous TGF-β, which can have deleterious consequences.[9−12]

Using phage display, we identified dodecapeptides that bind to the extracellular domains of both TβRI and TβRII to form complexes with $K_d \approx 10^{-5}$ M.[21] These peptides do not, however, antagonize the binding of TGF-β. In addition, we demonstrated that a multivalent display of these ligands on a polyethylene glycol (PEG)-based dendrimer increases their functional efficacy for the receptors.[21] Likewise, immobilization of the ligands on a synthetic surface enables activation by subpicomolar concentrations of endogenous TGF-β.[22] Gene expression profiles revealed that the surfaces regulate TGF-β-responsive genes selectively. Now, we sought to exploit these ligands in vivo.

Collagen is the major component of the extracellular matrix (ECM).[23−25] We and others have reported on the use of collagen-mimetic peptides (CMPs) to anchor probes and growth factors in damaged or abnormal collagen.[26−35] Here, we use a CMP conjugate to immobilize a peptidic ligand for TGF-β receptors in wound beds of mice. Our intent is to cluster cell−surface TβRI and TβRII and thereby enhance the sensitivity of cells to circulating TGF-β (Figure 1B). As TGF-β is involved in various stages of wound healing,[9−12] we validate the efficacy of our approach by using a variety of assays.

Received: September 22, 2021
Accepted: January 12, 2022
Published: January 27, 2022

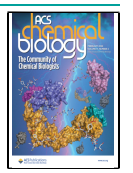

https://doi.org/10.1021/acschembio.1c00745
ACS Chem. Biol. 2022, 17, 314−321

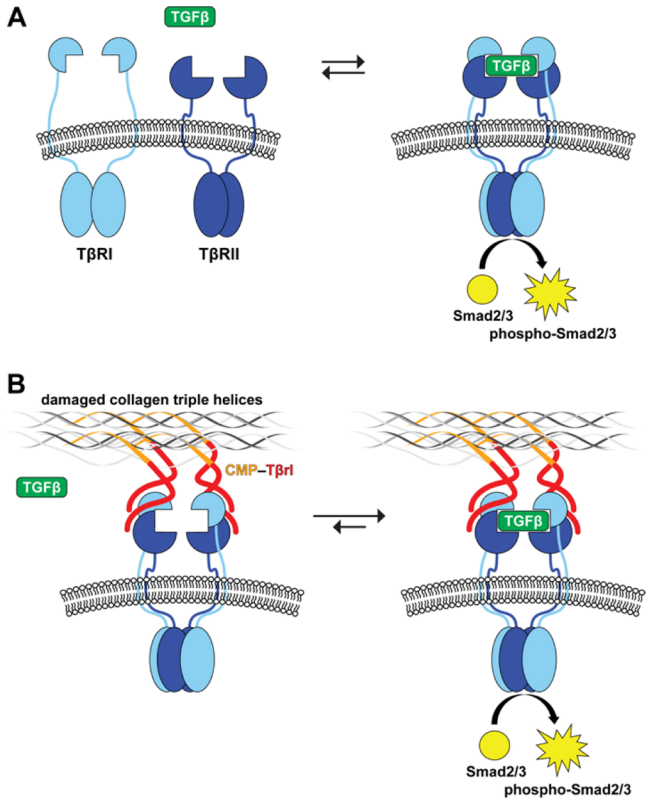

Figure 1. Representation of TGF-β receptor–ligand complex formation and its activation of the Smad2/3 proteins by their cytosolic kinase domains. (A) TGF-β induces the heterotetramerization of type-I and type-II receptors (TβRI and TβRII). (B) Clustering of TβRI and TβRII by binding to a ligand (**Tβrl**) that is immobilized in a wound bed upon the annealing of a pendant **CMP**.

RESULTS AND DISCUSSION

Peptide Design. As an effector to sensitize cell–surface receptors to TGF-β signaling, we used the LTGKNFPMFHRN peptide.[21] As a CMP, we chose $(PPG)_7$ because of its simplicity and demonstrated efficacy in relevant contexts in vitro, ex vivo, and in vivo.[26,28,30,33,34] (We note that the use of a CMP containing 4-fluoroproline residues could be advantageous in future studies.[29,31,36]) In its initial discovery, LTGKNFPMFHRN (**Tβrl**) was displayed as a fusion to the N-terminus of the PIII coat protein of the phage.[21] We mimicked this display by conjugating **Tβrl** to the N-terminus of **CMP**. Accordingly, we synthesized the 33-mer peptide **Tβrl–CMP** and its **Tβrl** and **CMP** components by solid-phase peptide synthesis (SPPS).

Mouse Model. Wound healing is a complex process. Mouse models have illuminated the mechanisms that underlie wound healing and established translatable therapeutic strategies.[37−40] We chose to use diabetic (*db*/*db*) mice as our model. These mice exhibit characteristics similar to those of adult human onset type II diabetes mellitus,[41,42] including impaired wound healing.[43] Excisional wounds in *db*/*db* mice show a delay in wound closure, decreased granulation tissue formation, decreased vascularization in the wound bed, and diminished cell proliferation.[44] The course of wound healing in these mice follows closely the clinical observations of human diabetic patients.[45] For example, these mice show delayed and reduced expression of keratinocyte growth factor and peripheral neuropathy,[46] as do diabetic humans.[47]

We employed an excisional wound model, which heals from the wound margins and provides the broadest assessment of the various parameters for wound healing, such as re-epithelialization, fibrovascular proliferation, contracture, and angiogenesis.[38] This wound model also offers large dorsal surfaces that simplify the application of topical agents directly into the wound bed and provides two wounds side-by-side on the same mouse.

Unsplinted Wounds. Wounds were created in the craniodorsal region of d*b*/d*b* mice under anesthesia and treated topically with **Tβrl–CMP** (25 μL of a 20 mM solution in 5% PEG/saline solution).[48,49] **CMP** and **Tβrl** (25 μL of 20 mM solutions in 5% PEG/saline) were also tested individually. The delivery vehicle itself was tested as a control.

The fibrovascular influx and the deposition of new collagen in wounds were measured by examining the picrosirius red-stained histologic sections under polarized light[50] and expressed as a percentage of the total wound area. The picrosirius red stain highlights the areas of new collagen deposition, as well as extant dermal collagen. Due to more extensive cross-linking and maturation, older collagen is stained more brightly and densely in comparison to newly formed collagen. Upon its release from degranulating platelets, TGF-β1 can attract fibroblasts chemotactically to a wound site[51−53] and stimulate their proliferation.[54] As part of a

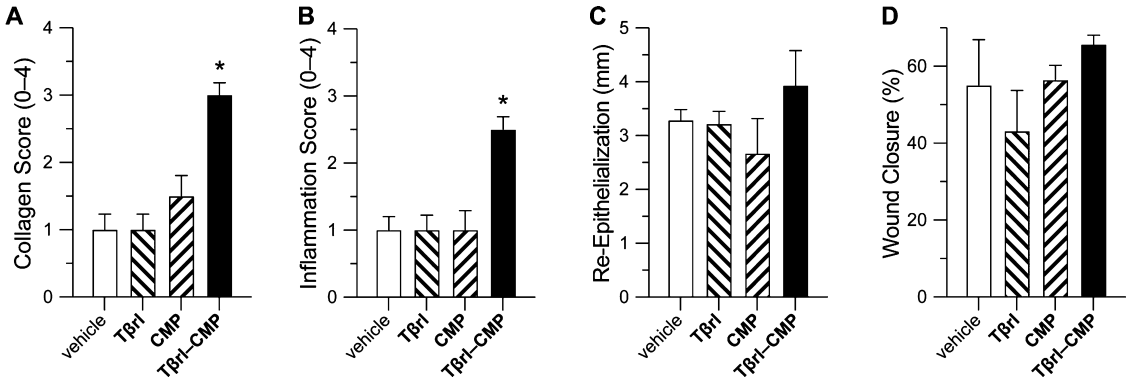

Figure 2. Effect of **Tβrl–CMP** (0.5 μmol) and controls on the healing of unsplinted cutaneous wounds in mice. Values are the mean ± SE (n = 10 wounds in 5 mice) with *p < 0.05. (A) Fibrovascular influx in wounds on a scale of 0–4 on day 12 post-surgery. (B) Inflammation in wounds on a scale of 0–4 on day 12 post-surgery. (C) Re-epithelialization of wounds on day 16 post-surgery. (D) Wound closure on day 12 post-surgery, calculated as the wound size as a percentage of the original wound size on day 0.

https://doi.org/10.1021/acschembio.1c00745
ACS Chem. Biol. 2022, 17, 314−321

positive feedback mechanism, fibroblasts release additional TGF-β in response and promote collagen biosynthesis.

Compared to the control wounds treated with **Tβrl**, **CMP**, or the delivery vehicle, wounds exposed to **Tβrl−CMP** exhibited a significant increase in the amount of collagen deposited in the wound bed (Figure 2A). This result is consistent with reports in which topical application of TGF-β in animal models enhanced the production of collagen and fibronectin by fibroblasts[55,56] and potently stimulated granulation tissue formation in wound-healing models.[57,58] In contrast, the production of collagen was diminished in the presence of anti−TGF-β antibodies.[59]

The wound-healing process is associated with the transient accumulation of fibroblasts that express elevated levels of TβRI and TβRII.[15−20] The highest cellular density is observed in the deepest regions of the granulation tissue.[60] **Tβrl−CMP** tethered to the wound bed is poised to preorganize these receptors and thereby enhance the cellular sensitivity to endogenous TGF-β signaling and the consequent formation of new collagen, without a need for exogenous TGF-β (Figure 1). Earlier work showed that tethering TGF-β to a PEG-based polymer scaffold caused a significant increase in matrix production and collagen deposition.[61] Such a treatment also counteracted the attenuation of ECM production, which is observed otherwise in the presence of biomaterials containing cell-adhesive ligands.[62] The **Tβrl−CMP** conjugate can behave in a similar manner and promote cellular adhesion while strengthening the wound bed itself by enhancing collagen synthesis and consequent ECM production. **Tβrl** alone cannot, however, access such preorganization and provides a response that is indistinguishable from that of the delivery vehicle (Figure 2A).

A similar outcome was apparent when wounds were analyzed for an inflammatory response. The concentration of TGF-β is ∼1 pM in human serum.[63] Upon cutaneous injury, TGF-β levels elevate rapidly.[64,65] For example, TGF-β levels reach a peak at 3 days post 6 mm full-thickness wounding in transgenic mice, which coincides with the peak of the inflammation during early stages of wound healing.[65] Subcutaneous injection of TGF-β affords a histological pattern for neutrophil and macrophage recruitment, fibroblast proliferation, and vascular growth, similar to the process of normal inflammation and repair in cutaneous wounds.[57] In early stages, TGF-β is a highly chemotactic ligand for human peripheral blood monocytes,[66] which is critical for the initiation of an inflammatory response. Through a positive feedback mechanism, the recruited monocytes and macrophages produce more TGF-β (thereby perpetuating their activation) as well as mitogenic and chemotactic substances that act on other cells. Wounds treated with **Tβrl−CMP** showed an inflammatory influx significantly greater than that of **Tβrl**, **CMP**, or the delivery vehicle (Figure 2B). The macrophages once activated or during maturation down-regulate their receptors for TGF-β and hence their ability to be stimulated further.[66] The peripheral blood monocytes also become susceptible to deactivation by TGF-β,[67] which inhibits the proteolytic environment created by inflammatory cells and eases the healing process into a proliferative phase.[68]

Re-epithelialization is the process by which keratinocytes both proliferate and migrate from the wound edges to create a barrier over the wound.[69] The role of TGF-β in this process is not completely understood. In vitro, TGF-β inhibits the proliferation of keratinocyte but enhances their migration.[70,71]

In Vivo Data Are Contradictory. Transgenic mice that overproduced TGF-β show enhanced epithelialization in partial-thickness wounds,[72] and anti−TGF-β antibodies administered to rabbits impair epithelialization.[73] On the other hand, mice null for Smad3 show accelerated keratinocyte proliferation and epithelialization upon the administration of TGF-β compared to wild-type mice.[52,74] In our experiment, we observed a tendency toward increased epithelialization of wound beds treated with **Tβrl−CMP** (Figure 2C). This result is consistent with cells responding quickly to endogenous TGF-β, which modulates the proliferative and migratory properties of the keratinocytes.[70,71]

No discernible differences were apparent in the rate of wound closure in the treated wounds (Figure 2D). This equivalence could be due to the preponderance of wound closure by contracture in rodents. That obscures wound changes related to epithelial closure or from the formation of scabs, whose removal disturbs the newly formed epidermis and could make wound size measurements inconclusive. We therefore took an alternative, complementary experimental approach.

Splinted Wounds. Mouse skin models are informative but dissimilar from human skin models in that their major mechanism of wound closure is contraction; in humans, re-epithelialization and granulation tissue formation are the major phases.[37−40,69] The use of splints around excisional wounds in mice forces healing to occur by granulocyte formation and re-epithelialization while minimizing the effects of contraction compared to those in unsplinted wound models.[75] As described previously,[28] we sutured silicone O-rings around the wound margins to act as splints. We increased the cohort size to eight mice per group. Wounds were treated with 25 μL of **Tβrl−CMP**, **Tβrl**, **CMP**, or the delivery vehicle, as with the unsplinted wounds. The wounded mice were then allowed to recover and monitored over a period of 16 days.

Histopathological analysis post-euthanasia on day 16 revealed that 15 of the 16 wounds treated with **Tβrl−CMP** were closed completely (Figure 3). Likewise, the wound size

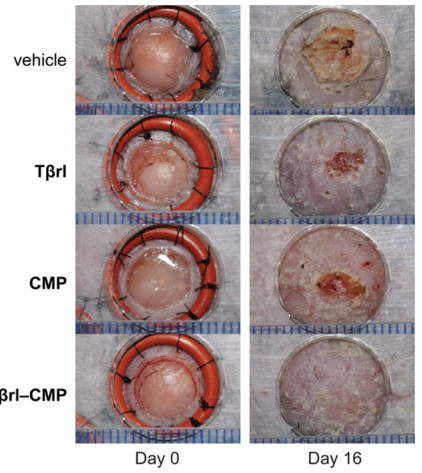

Figure 3. Representative images of splinted wounds in mice on day 0 (i.e., immediately post-surgery) and on day 16 post-surgery after the removal of splints but before euthanasia. Wounds were treated with vehicle (5% PEG/saline), **Tβrl** (0.5 μmol), **CMP** (0.5 μmol), or **Tβrl−CMP** (0.5 μmol). In mice treated with **Tβrl−CMP**, 15 of the 16 wounds showed complete closure. Scale bars (blue) are separated by 1.0 mm.

https://doi.org/10.1021/acschembio.1c00745
ACS Chem. Biol. 2022, 17, 314−321

was significantly lower than that for the delivery vehicle (Figure 4A). Treatment with **Tβrl** also showed a slightly

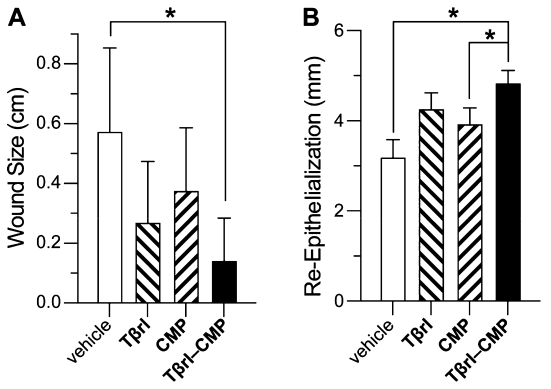

Figure 4. Effect of **Tβrl–CMP** (0.5 μmol) and controls on the healing of splinted cutaneous wounds in mice. (A) Wound closure on day 16 post-surgery, represented as the distance between the advancing edges at the widest diameter. (B) Re-epithelialization of wounds on day 16 post-surgery. Values are the mean ± SE (n = 16 wounds in 8 mice) with *p < 0.05.

enhanced wound closure, though it was not significantly different than that for the delivery vehicle and comparable to that for treatment with **CMP**. Upon comparing the extent of re-epithelialization, we noticed improved keratinocyte proliferation in the wound beds treated with **Tβrl–CMP** in comparison to that in the wounds treated with **CMP** or the delivery vehicle (Figure 4B). TGF-β has been reported to promote epithelial cell attachment and migration in vivo[76,77] and to stimulate the expression of keratinocyte integrins during re-epithelialization.[78] Keratinocyte migration takes place across a substrate, typically the dermis. The deposition of a substantial granulation tissue layer over the longer time period of the splinted-wound experiments (16 days) could have provided the requisite surface for the migration of keratinocytes and increased the length of the newly formed epithelial layer.

Dose–Response Analyses. Finally, we assessed the potency of the TGF-β receptor ligand in the ECM formation by treating the wounds with increasing doses of **Tβrl–CMP**. Identical 6 mm o.d. wounds were created on the backs of *db/db* mice (5 mice/10 wounds per group) and then treated with a 25 μL solution of **Tβrl–CMP** (0.080–50 mM) for 30 min. The mice were allowed to recover, and the wounds were analyzed after 12 days. The amount of newly formed collagen in the wound bed was identified with picrosirius red stain and expressed as a percentage of the marked area at a depth of 0.75 mm from the healed surface.

The extent to which collagen was deposited was comparable in the wounds treated with 0.08, 0.4, 2.0, and 10.0 mM solutions but increased in wounds treated with 50 mM **Tβrl–CMP** (Figure 5A). These data were mirrored in the histopathological analyses (Figure 6).

Wound re-epithelialization did not exhibit a marked dependence on the **Tβrl–CMP** dose, though there seemed to be a tendency for a higher response upon treatment with higher doses (Figure 5B). The inflammatory response was reflected in the presence of mononuclear cells in larger amounts in wounds treated with higher doses than in wounds treated with lower doses, which retained discernible amounts of neutrophils and polymorphonuclear cells.

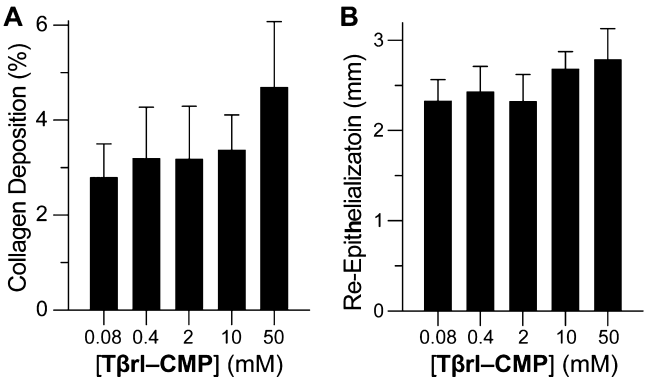

Figure 5. Dose–response analysis of unsplinted cutaneous wounds in mice to **Tβrl–CMP** and controls. Wounds were treated with a 25 μL solution of **Tβrl–CMP** in 5% PEG/saline and analyzed on day 12 post-surgery. Values are the mean ± SE (n = 16 wounds in 8 mice). (A) New collagen deposition at a depth of 0.75 mm from the healed surface. (B) Re-epithelialization of wounds.

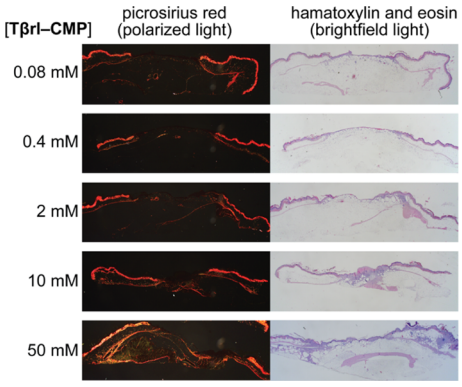

Figure 6. Representative histological images of **Tβrl–CMP**-treated wounds on day 12 post-surgery. Wounds were stained with picrosirius red and imaged with polarized light or stained with hematoxylin and eosin and imaged with brightfield light.

CONCLUSIONS

A **Tβrl–CMP** conjugate can upregulate collagen formation in mice. This result along with in vitro data[21,22] are consistent with its clustering of TGF-β receptors and thereby sensitizing cells to endogenous TGF-β. This mode of action is unique for a pendant on a CMP that is annealed to a wound bed and provides opportunities. The closure of severe wounds where viable tissue has been destroyed by trauma involves the deposition of new collagen in accordance with the severity of the damage. The amplified TGF-β activity during the initial stages of the wound healing process stimulates fibroblast proliferation and activity, as well as keratinocyte migration over the surface of the wounds. These actions accelerate the closure of wounds and the acquisition of tensile strength. Dose–response studies suggest that the amount of collagen deposition can be regulated without substantial changes in the rate of re-epithelialization. This type of healing could elicit scar formation yet could provide an effective means to treat severe damage, as incurred from third- or fourth-degree burns or traumatic mechanical damage, which might otherwise lead to lifelong impairment.

https://doi.org/10.1021/acschembio.1c00745
ACS Chem. Biol. 2022, 17, 314–321

EXPERIMENTAL PROCEDURES

Materials. Commercial chemicals were of reagent grade or better and were used without further purification. Anhydrous solvents were obtained from CYCLE-TAINER solvent delivery systems from J. T. Baker. High-performance liquid chromatography (HPLC)-grade solvents were obtained in sealed bottles from Fisher Chemical. In all reactions involving anhydrous solvents, glassware was either oven- or flame-dried. Polyethylene glycol 8000 (PEG) from Fisher Chemical and bacteriostatic saline (0.9% w/v sodium chloride) from Hospira were used to prepare 5% w/v PEG in saline solution as a delivery vehicle for treatments.

Male mice (n = 92) (BKS.Cg-*Dock7*^{m} +/+ *Lepr*^{db}/J) were from The Jackson Laboratory. Isoflurane was from Abbott Laboratories, buprenorphine·HCl was from Reckitt Benckiser, and chlorhexidine gluconate (4% w/v) was from Purdue Products. Silicone O-rings (15 mm o.d., 11 mm i.d., 2 mm thickness) were from McMaster Carr.

Instrumentation. Semi-preparative HPLC was performed using a Varian Dynamax C-18 reversed-phase column. Analytical HPLC was performed using a Vydac C-18 reversed-phase column. Mass spectrometry was performed using an Applied Biosystems Voyager DE-Pro matrix-assisted laser desorption/ionization mass spectrometer from Life Technologies at the Biophysics Instrumentation Facility at the University of Wisconsin−Madison.

Peptide Synthesis and Purification. Peptides were synthesized by SPPS using a 12-channel Symphony peptide synthesizer from Protein Technologies at the University of Wisconsin−Madison Biotechnology Center. Peptides were synthesized on Novabiochem FmocGly-Wang resin (0.4−0.7 mmol g^{-1}, 100−200 mesh) from EMD Chemicals. Amino acids were converted to active esters by treatment with 1-hydroxybenzotriazole (HOBt, 3 equiv), *O*-benzotriazole-*N*,*N*,*N*′,*N*′-tetramethyl-uronium-hexafluoro-phosphate (3 equiv), and *N*-methylmorpholine (HBTU, 6 equiv). Fmoc-deprotection was achieved by treatment with piperidine (NMM, 20% v/v) in dimethylformamide.

CMP and **T*β*rl−CMP** were synthesized by the sequential coupling of FmocProOH and FmocProProGlyOH. A proline residue was coupled to the FmocGly-Wang resin after a swell cycle, and the next seven residues were installed by using excess (5 equiv) FmocProOH, FmocProProGlyOH (which was synthesized as reported previously[79]), FmocAsn(Trt)OH, FmocArg(Pbf)OH, FmocHis(Trt)OH, FmocPheOH, FmocMetOH, FmocLys(Boc)OH, FmocGlyOH, FmocThr(*t*Bu)OH, and FmocLeuOH. **CMP** was cleaved from the resin by using 95:2.5:2.5 trifluoroacetic acid (TFA)/triisopropylsilane/water (total volume: 2 mL); **T*β*rl−CMP** was cleaved from the resin by using 92.5:5:2.5 TFA/thioanisole/ethanedithiol (total volume: 2 mL). Both peptides were precipitated from *t*-butylmethylether at 0 °C, isolated by centrifugation, and purified by semi-preparative HPLC using linear gradients: **CMP**, 5−85% v/v B over 45 min and **T*β*rl−CMP**, 10−90% v/v B over 50 min. Solvent A was H_2O containing TFA (0.1% v/v); solvent B was CH_3CN containing TFA (0.1% v/v). **CMP** was readily soluble in water, but **T*β*rl−CMP** required the addition of CH_3CN (20% v/v) to form a clear solution for HPLC analysis. All peptides were judged to be >90% pure by HPLC and matrix-assisted laser desorption/ionization time-of-flight (MALDI−TOF) mass spectrometry: (m/z) $[M + H]^+$ calcd for **CMP**, 1777; found 1777; (m/z) $[M + H]^+$ calcd for **T*β*rl−CMP**, 3221; found 3221.

T*β*rl was either obtained from Biomatik or synthesized at the Peptide Synthesis Facility on Fmoc-Asn(Trt)-Wang resin (0.54 mmol g^{-1}, 100−200 mesh; Novabiochem, EMD Chemicals).

Mouse Models. Mice aged 8−12 weeks were housed in groups until the day of surgery and then in separate cages post-surgery. The experimental protocol followed was according to the guidelines issued by the Institutional Animal Care and Use Committee at the University of Wisconsin−Madison. Mice were provided food and water ad libitum, as well as enrichment, and housed in a temperature-controlled environment with 12 h light and dark cycles.

On the day of the surgery, mice were anaesthetized with isoflurane gas using an induction chamber. For pain management, buprenorphine·HCl (0.01 mg mL^{-1} in 0.9% w/v saline) was injected subcutaneously (0.4 mL per mouse). Eyes were lubricated, and hind nails were clipped. The craniodorsal region was shaved using electric clippers, and the shaved area was scrubbed with alternating cotton swabs of chlorhexidine and sterile saline in circular strokes. Residual hair was removed. For the unsplinted wound model, identical 8 mm wounds were created on each side of the body with a biopsy punch, and the wounding was completed using forceps and scissors to prevent the punch from lacerating the subcutaneous tissue. The wounds were treated with **T*β*rl−CMP** or controls and then allowed to incubate for 30 min while the mouse was still under anesthesia. Wounds were photographed, and the mice were then allowed to recover in their cages. For the dose−response experiments, unsplinted wounds were created with a 6 mm biopsy punch and then treated with 25 μL of the delivery vehicle containing increasing concentrations of **T*β*rl−CMP**, followed by incubation for 30 min under anesthesia.

For the splinted wound model, splints were bilaterally placed in a symmetrical arrangement using an adhesive and then secured to the skin using eight interrupted 5−0 nylon sutures, encircling the splints with the knots.[80] Wounds were created in the center of the splints using an 8 mm biopsy punch and then removing the skin using forceps and scissors. The wounds were then treated with **T*β*rl−CMP** or controls and allowed to incubate for 30 min while the mouse was still under anesthesia. The wounds were photographed, and the mice were allowed to recover on a warming pad. ImageJ software[81] from the National Institutes of Health was used to calculate the wound area (mm^2) from digital photographs. Wound closure was defined as the reduction in the area between the wound edges over the course of the study and was reported as a percentage of the original wound size.

Mice were monitored daily for behavioral changes, and their body weights were recorded on days 1, 3, 6, 9, 12, and 16. The splints were checked daily, and any broken or untied suture was replaced according to the experimental protocol (vide supra). If only one suture was compromised during a 24 h period, it was replaced with a new suture. If, however, two or more sutures were compromised during a 24 h period, the wound was no longer considered splinted and was removed from the study.

Wound Harvesting. Histopathology cassettes were labeled for mouse and wound identification. Note cards (1 in. × 1 in. square) were fitted to the bottom of the histopathology cassettes, and one edge was labeled "cranial" and aligned with the cranial side of the harvested wound. On the final day of the experiment, mice were euthanized using Beuthanasia-D (0.5 mL per mouse). Using a scalpel blade and scissors, a 3/4 in. × 3/4 in. square area of the tissue was taken from the mouse, keeping the wound centered in the tissue section. Deep dissection was performed to harvest several layers of tissue deep in the wound. The square section of tissue was affixed to the note card, with the cranial edge aligned with the labeled edge of the card. The cassettes were then closed and placed in formalin-filled jars for histopathological analysis.

Histopathological Analyses. After euthanasia, the entire wound bed as well as the intact skin margin >5 mm was excised to the retroperitoneum. The harvested tissue was fixed in 10% v/v formalin for at least 24 h and then sectioned through the center of the lesion. The center was marked with India ink prior to the fixation. Routine paraffin processing was performed, and the tissue samples were sectioned serially at a thickness of 5 μm, ensuring that the center of the lesion was included on the slide. The slides were then stained with hematoxylin and eosin and with picrosirius red. Sections were photographed under a light microscope using a mounted DP72 digital camera from Olympus. The size of the wound, length of re-epithelialization, amount of fibrovascular proliferation in the dermis, and inflammatory response were measured on the slides containing the center of the lesion, and images were analyzed using CellScience Dimension 1.4 software from Olympus. The size of the wound was defined as the area of the wound not covered by an advancing epithelial layer and was calculated by measuring the distance between the opposite free edges of the wound. The length of re-epithelialization was defined as the length of the layer of proliferating

https://doi.org/10.1021/acschembio.1c00745
ACS Chem. Biol. 2022, 17, 314−321

keratinocytes covering the wound area and was calculated by measuring the distance between the free edge of the keratinocyte layer and the base where the cells were still associated with the native dermal tissue. Both sides of the lesion were measured, and the final result was the sum of the two measurements. For wounds that had undergone complete re-epithelialization, a single measurement was taken from base to base.

Fibrovascular dermal proliferation was measured by examining the picrosirius red-stained sections under polarized light, which highlighted the newly deposited dermal collagen. CellScience Dimension 1.4 software was used to select the wound bed; the amount of new collagen in the selected area was measured and expressed as a percentage of the total wound area or using a semi-quantitative histopathological 0−4 scoring system, where 0 indicated no discernible collagen formation, 1 indicated that <25% of the wound area was covered with fresh collagen, 2 indicated that 25−50% of the wound area was covered with fresh collagen, 3 indicated that 50−75% of the wound area was covered with fresh collagen, and 4 indicated that >75% of the wound area was covered with fresh collagen. The inflammatory response was assessed using a semi-quantitative histopathological 0−4 scoring system, where 0 indicated no inflammation, 1 indicated that <25% of the wound area was affected, 2 indicated that 25−50% of the wound area was affected, 3 indicated that 50−75% of the wound area was affected, and 4 indicated that >75% of the wound area was affected. The inflammatory response was also categorized as "acute" when >75% of the cells were neutrophils, "chronically active" when there was a 1:1 ratio of neutrophils and mononuclear cells, and "chronic" when >75% of the inflammatory cells were mononuclear.

Statistical Analyses. All data were analyzed using a Mann−Whitney rank sum test, and statistical significance was set as $p < 0.05$. Statistical analyses were executed using Prism Version 5.0 software from GraphPad Software.

AUTHOR INFORMATION

Corresponding Author

Ronald T. Raines − *Department of Chemistry, University of Wisconsin−Madison, Madison, Wisconsin 53706, United States; Department of Biochemistry, University of Wisconsin−Madison, Madison, Wisconsin 53706, United States; Department of Chemistry, Massachusetts Institute of Technology, Cambridge, Massachusetts 02139, United States;* orcid.org/0000-0001-7164-1719; Email: rtraines@mit.edu

Authors

Sayani Chattopadhyay − *Department of Chemistry, University of Wisconsin−Madison, Madison, Wisconsin 53706, United States*

Leandro B. C. Teixeira − *Department of Pathobiological Sciences, School of Veterinary Medicine, University of Wisconsin−Madison, Madison, Wisconsin 53706, United States;* orcid.org/0000-0001-9960-678X

Laura L. Kiessling − *Department of Chemistry, University of Wisconsin−Madison, Madison, Wisconsin 53706, United States; Department of Biochemistry, University of Wisconsin−Madison, Madison, Wisconsin 53706, United States; Department of Chemistry, Massachusetts Institute of Technology, Cambridge, Massachusetts 02139, United States;* orcid.org/0000-0001-6829-1500

Jonathan F. McAnulty − *Department of Surgical Sciences, School of Veterinary Medicine, University of Wisconsin−Madison, Madison, Wisconsin 53706, United States*

Complete contact information is available at: https://pubs.acs.org/10.1021/acschembio.1c00745

Funding

This work was supported by grants RC2 AR058971, R56 AR044276, R01 AI055258, and R01 GM049975 (NIH). MALDI−TOF mass spectrometry was performed at the University of Wisconsin−Madison Biophysics Instrumentation Facility, which was established with grants BIR-9512577 (NSF) and S10 RR013790 (NIH).

Notes

The authors declare no competing financial interest.

ACKNOWLEDGMENTS

We are grateful to L. Li and N. L. Abbott for their guidance and advice. We thank P. Kierski, D. Calderon, D. Tackes, K. Johnson, and Z. Joseph for help with the wound surgery and animal care.

ABBREVIATIONS

CMP, collagen-mimetic peptide [here, $(PPG)_7$]; TGF-β, transforming growth factor-β; **Tβrl−CMP**, collagen-mimetic peptide−transforming growth factor-β receptor ligand conjugate [here, LTGKNFPMFHRN−$(PPG)_7$]; **TβRI**, transforming growth factor-β type-1 receptor; **TβRII**, transforming growth factor-β type-2 receptor; **Tβrl**, transforming growth factor-β receptor ligand (here, LTGKNFPMFHRN)

REFERENCES

(1) Massagué, J. TGF-β signal transduction. *Annu. Rev. Biochem.* **1998**, *67*, 753−791.

(2) Shi, Y.; Massagué, J. Mechanisms of TGF-β signaling from cell membrane to the nucleus. *Cell* **2003**, *113*, 685−700.

(3) Massagué, J. TGF β signalling in context. *Nat. Rev. Mol. Cell Biol.* **2012**, *13*, 616−630.

(4) Meng, X.-m.; Nikolic-Paterson, D. J.; Lan, H. Y. TGF-β: The master regulator of fibrosis. *Nat. Rev. Nephrol.* **2016**, *12*, 325−338.

(5) Wrana, J. L.; Attisano, L.; Cárcamo, J.; Zentella, A.; Doody, J.; Laiho, M.; Wang, X.-F.; Massague, J. TGF-β signals through a heteromeric protein kinase receptor complex. *Cell* **1992**, *71*, 1003−1014.

(6) Hart, P. J.; Deep, S.; Taylor, A. B.; Shu, Z.; Hinck, C. S.; Hinck, A. P. Crystal structure of the human TβR2 ectodomain−TGFβ3 complex. *Nat. Struct. Biol.* **2002**, *9*, 203−208.

(7) Heldin, C.-H.; Moustakas, A. Signaling receptors for TGF-β family members. *Cold Spring Harb. Perspect. Biol.* **2016**, *8*, a022053.

(8) Schiller, M.; Javelaud, D.; Mauviel, A. TGF-β-induced SMAD signaling and gene regulation: Consequences for extracellular matrix remodeling and wound healing. *J. Dermatol. Sci.* **2004**, *35*, 83−92.

(9) Faler, B. J.; Macsata, R. A.; Plummer, D.; Mishra, L.; Sidawy, A. N. Transforming growth factor-β and wound healing. *Perspect. Vasc. Surg. Endovasc. Ther.* **2006**, *18*, 55−62.

(10) Prud'homme, G. J. Pathobiology of transforming growth factor β in cancer, fibrosis and immunologic disease, and therapeutic considerations. *Lab. Invest.* **2007**, *87*, 1077−1091.

(11) Pakyari, M.; Farrokhi, A.; Maharlooei, M. K.; Ghahary, A. Critical role of transforming growth factor beta in different phases of wound healing. *Adv. Wound Care (New Rochelle)* **2013**, *2*, 215−224.

(12) Liarte, S.; Bernabé-García, Á.; Nicolás, F. J. Role of TGF-β in skin chronic wounds: A keratinocyte perspective. *Cells* **2020**, *9*, 306.

(13) Henderson, N. C.; Rieder, F.; Wynn, T. A. Fibrosis: From mechanisms to medicines. *Nature* **2020**, *587*, 555−566.

(14) Pandit, A.; Ashar, R.; Feldman, D. The effect of TGF-β delivered through a collagen scaffold on wound healing. *J. Invest. Surg.* **1999**, *12*, 89−100.

(15) Mustoe, T. A.; Pierce, G. F.; Thomason, A.; Gramates, P.; Sporn, M. B.; Deuel, T. F. Accelerated healing of incisional wounds in rats induced by transforming growth factor-β. *Science* **1987**, *237*, 1333−1336.

(16) Broadley, K. N.; Aquino, A. M.; Hicks, B.; Ditesheim, J. A.; McGee, G. S.; Demetriou, A. A.; Woodward, S. C.; Davidson, J. M. The diabetic rat as an impaired wound healing model: Stimulatory effects of transforming growth factor-β and basic fibroblast growth factor. *Biotechnol. Therapeut.* **1989**, *1*, 55−68.
(17) Ammann, A. J.; Beck, L. S.; DeGuzman, L.; Hirabayashi, S. E.; Pun Lee, W.; McFatridge, L.; Nguyen, T.; Xu, Y.; Mustoe, T. A. Transforming growth factor-β effect on soft tissue repair. *Ann. N.Y. Acad. Sci.* **1990**, *593*, 124−134.
(18) Ksander, G. A.; Chu, G. H.; McMullin, H.; Ogawa, Y.; Pratt, B. M.; Rosenblatt, J. S.; McPherson, J. M. Transforming growth factors-β1 and β2 enhance connective tissue formation in animal models of dermal wound healing by secondary intent. *Ann. N.Y. Acad. Sci.* **1990**, *593*, 135−147.
(19) Ksander, G. A.; Gerhardt, C. O.; Olsen, D. R. Exogenous transforming growth factor-β2 enhances connective tissue formation in transforming growth factor-β1—deficient, healing-impaired dermal wounds in mice. *Wound Rep. Regen.* **1993**, *1*, 137−148.
(20) Beck, L. S.; DeGuzman, L.; Lee, W. P.; Xu, Y.; Siegel, M. W.; Amento, E. P. One systemic administration of transforming growth factor-beta 1 reverses age- or glucocorticoid-impaired wound healing. *J. Clin. Invest.* **1993**, *92*, 2841−2849.
(21) Li, L.; Orner, B. P.; Huang, T.; Hinck, A. P.; Kiessling, L. L. Peptide ligands that use a novel binding site to target both TGF-β receptors. *Mol. Biosyst.* **2010**, *6*, 2392−2402.
(22) Li, L.; Klim, J. R.; Derda, R.; Courtney, A. H.; Kiessling, L. L. Spatial control of cell fate using synthetic surfaces to potentiate TGF-β signaling. *Proc. Natl. Acad. Sci. U.S.A.* **2011**, *108*, 11745−11750.
(23) Shoulders, M. D.; Raines, R. T. Collagen structure and stability. *Annu. Rev. Biochem.* **2009**, *78*, 929−958.
(24) Chattopadhyay, S.; Raines, R. T. Collagen-based biomaterials for wound healing. *Biopolymers* **2014**, *101*, 821−833.
(25) Bella, J.; Hulmes, D. J. S. Fibrillar collagen. *Subcell. Biochem.* **2017**, *82*, 457−490.
(26) Chattopadhyay, S.; Murphy, C. J.; McAnulty, J. F.; Raines, R. T. Peptides that anneal to natural collagen in vitro and ex vivo. *Org. Biomol. Chem.* **2012**, *10*, 5892−5897.
(27) Wahyudi, H.; Reynolds, A. A.; Li, Y.; Owen, S. C.; Yu, S. M. Targeting collagen for diagnostic imaging and therapeutic delivery. *J. Controlled Release* **2016**, *240*, 323−331.
(28) Chattopadhyay, S.; Guthrie, K. M.; Teixeira, L.; Murphy, C. J.; Dubielzig, R. R.; McAnulty, J. F.; Raines, R. T. Anchoring a cytoactive factor in a wound bed promotes healing. *J. Tissue Eng. Regener. Med.* **2016**, *10*, 1012−1020.
(29) Bennink, L. L.; Li, Y.; Kim, B.; Shin, I. J.; San, B. H.; Zangari, M.; Yoon, D.; Yu, S. M. Visualizing collagen proteolysis by peptide hybridization: From 3D cell culture to in vivo imaging. *Biomaterials* **2018**, *183*, 67−76.
(30) Ellison, A. J.; Raines, R. T. A pendant peptide endows a sunscreen with water-resistance. *Org. Biomol. Chem.* **2018**, *16*, 7139−7142.
(31) Dones, J. M.; Tanrikulu, I. C.; Chacko, J. V.; Schroeder, A. B.; Hoang, T. T.; Gibson, A. L. F.; Eliceiri, K. W.; Raines, R. T. Optimization of interstrand interactions enables burn detection with a collagen-mimetic peptide. *Org. Biomol. Chem.* **2019**, *17*, 9906−9912.
(32) Schroeder, A. B.; Karim, A.; Ocotl, E.; Dones, J. M.; Chacko, J. V.; Liu, A.; Raines, R. T.; Gibson, A. L. F.; Eliceiri, K. W. Optical imaging of collagen fiber damage to assess thermally injured human skin. *Wound Rep. Regen.* **2020**, *28*, 848−855.
(33) Ellison, A. J.; Tanrikulu, I. C.; Dones, J. M.; Raines, R. T. Cyclic peptide mimetic of damaged collagen. *Biomacromolecules* **2020**, *21*, 1539−1547.
(34) Ellison, A. J.; Dempwolff, F.; Kearns, D. B.; Raines, R. T. Role for cell-surface collagen of *Streptococcus pyogenes* in infections. *ACS Infect. Dis.* **2020**, *6*, 1836−1843.
(35) Song, J. Y.; Pineault, K. M.; Dones, J. M.; Raines, R. T.; Wellik, D. M. *Hox* genes maintain critical roles in the adult skeleton. *Proc. Natl. Acad. Sci. U.S.A.* **2020**, *117*, 7296−7304.
(36) Newberry, R. W.; Raines, R. T. 4-Fluoroprolines: Conformational analysis and effects on the stability and folding of peptides and proteins. *J. Heterocycl. Chem.* **2017**, *48*, 1−25.
(37) Davidson, J. M. Animal models for wound repair. *Arch. Dermatol. Res.* **1998**, *290*, S1−S11.
(38) Greenhalgh, D. G.; Warden, G. D. Wound Care Models. *Surgical Research*; Academic Press: London, UK, 2001; pp 379−391.
(39) Zomer, H. D.; Trentin, A. G. Skin wound healing in humans and mice: Challenges in translational research. *J. Dermatol. Sci.* **2018**, *90*, 3−12.
(40) Parnell, L. K. S.; Volk, S. W. The evolution of animal models in wound healing research: 1993−2017. *Adv. Wound Care (New Rochelle)* **2019**, *8*, 692−702.
(41) Coleman, D. L. Obese and diabetes: Two mutant genes causing diabetes-obesity syndromes in mice. *Diabetologia* **1978**, *14*, 141−148.
(42) Kämpfer, H.; Paulukat, J.; Mühl, H.; Wetzler, C.; Pfeilschifter, J.; Frank, S. Lack of interferon-ν production despite the presence of interleukin-18 during cutaneous wound healing. *Mol. Med.* **2000**, *6*, 1016−1027.
(43) Brem, H.; Tomiccanic, M.; Entero, H.; Hanflik, A.; Wang, V.; Fallon, J.; Ehrlich, H. The synergism of age and *db/db* genotype impairs wound healing. *Exp. Gerontol.* **2007**, *42*, 523−531.
(44) Michaels, J.; Churgin, S. S.; Blechman, K. M.; Greives, M. R.; Aarabi, S.; Galiano, R. D.; Gurtner, G. C. *db/db* Mice exhibit severe wound-healing impairments compared with other murine diabetic strains in a silicone-splinted excisional wound model. *Wound Rep. Regen.* **2007**, *15*, 665−670.
(45) Greenhalgh, D. G. Wound healing and diabetes mellitus. *Clin. Plast Surg.* **2003**, *30*, 37−45.
(46) Werner, S.; Breeden, M.; Hübner, G.; Greenhalgh, D. G.; Longaker, M. T. Induction of keratinocyte growth factor expression is reduced and delayed during wound healing in the genetically diabetic mouse. *J. Invest. Dermatol.* **1994**, *103*, 469−473.
(47) Norido, F.; Canella, R.; Zanoni, R.; Gorio, A. Development of diabetic neuropathy in the C57BL/Ks (*db/db*) mouse and its treatment with gangliosides. *Exp. Neurol.* **1984**, *83*, 221−232.
(48) Greenhalgh, D. G.; Sprugel, K. H.; Murray, M. J.; Ross, R. PDGF and FGF stimulate wound healing in the genetically diabetic mouse. *Am. J. Pathol.* **1990**, *136*, 1235−1246.
(49) Brown, R. L.; Breeden, M. P.; Greenhalgh, D. G. PDGF and TGF-α act synergistically to improve wound healing in the genetically diabetic mouse. *J. Surg. Res.* **1994**, *56*, 562−570.
(50) Dapson, R.; Fagan, C.; Kiernan, J.; Wickersham, T. Certification procedures for sirius red F3B (CI 35780, Direct red 80). *Biotech. Histochem.* **2011**, *86*, 133−139.
(51) Postlethwaite, A. E.; Keski-Oja, J.; Moses, H. L.; Kang, A. H. Stimulation of the chemotactic migration of human fibroblasts by transforming growth factor β. *J. Exp. Med.* **1987**, *165*, 251−256.
(52) Ashcroft, G. S.; Yang, X.; Glick, A. B.; Weinstein, M.; Letterio, J. J.; Mizel, D. E.; Anzano, M.; Greenwell-Wild, T.; Wahl, S. M.; Deng, C.; Roberts, A. B. Mice lacking Smad3 show accelerated wound healing and an impaired local inflammatory response. *Nat. Cell Biol.* **1999**, *1*, 260−266.
(53) Abe, R.; Donnelly, S. C.; Peng, T.; Bucala, R.; Metz, C. N. Peripheral blood fibrocytes: Differentiation pathway and migration to wound sites. *J. Immunol.* **2001**, *166*, 7556−7562.
(54) Lal, B. K.; Saito, S.; Pappas, P. J.; Padberg, F. T.; Cerveira, J. J.; Hobson, R. W.; Durán, W. N. Altered proliferative responses of dermal fibroblasts to TGF-β1 may contribute to chronic venous stasis ulcer. *J. Vasc. Surg.* **2003**, *37*, 1285−1293.
(55) Roberts, C. J.; Birkenmeier, T. M.; McQuillan, J. J.; Akiyama, S. K.; Yamada, S. S.; Chen, W. T.; Yamada, K. M.; McDonald, J. A. Transforming growth factor β stimulates the expression of fibronectin and of both subunits of the human fibronectin receptor by cultured human lung fibroblasts. *J. Biol. Chem.* **1988**, *263*, 4586−4592.
(56) Lynch, S. E.; Colvin, R. B.; Antoniades, H. N. Growth factors in wound healing. Single and synergistic effects on partial thickness porcine skin wounds. *J. Clin. Invest.* **1989**, *84*, 640−646.

https://doi.org/10.1021/acschembio.1c00745
ACS Chem. Biol. 2022, 17, 314−321

(57) Roberts, A. B.; Sporn, M. B.; Assoian, R. K.; Smith, J. M.; Roche, N. S.; Wakefield, L. M.; Heine, U. I.; Liotta, L. A.; Falanga, V.; Kehrl, J. H. Transforming growth factor type β: Rapid induction of fibrosis and angiogenesis in vivo and stimulation of collagen formation in vitro. *Proc. Natl. Acad. Sci. U.S.A.* **1986**, *83*, 4167−4171.
(58) Roberts, A. B. Transforming growth factor-β: activity and efficacy in animal models of wound healing. *Wound Rep. Regen.* **1995**, *3*, 408−418.
(59) Roberts, A. B.; Piek, E.; Böttinger, E. P.; Ashcroft, G.; Mitchell, J. B.; Flanders, K. C. Is Smad3 a major player in signal transduction pathways leading to fibrogenesis? *Chest* **2001**, *120*, S43−S47.
(60) Schmid, P.; Itin, P.; Cherry, G.; Bi, C.; Cox, D. A. Enhanced expression of transforming growth factor-β type I and type II receptors in wound granulation tissue and hypertrophic scar. *Am. J. Pathol.* **1998**, *152*, 485−493.
(61) Mann, B. K.; Schmedlen, R. H.; West, J. L. Tethered-TGF-β increases extracellular matrix production of vascular smooth muscle cells. *Biomaterials* **2001**, *22*, 439−444.
(62) Mann, B.; Tsai, A. T.; Scott-Burden, T.; West, J. L. Modification of surfaces with cell adhesion peptides alters extracellular matrix deposition. *Biomaterials* **1999**, *20*, 2281−2286.
(63) Slevin, M.; Krupinski, J.; Slowik, A.; Kumar, P.; Szczudlik, A.; Gaffney, J. Serial measurement of vascular endothelial growth factor and transforming growth factor-β1 in serum of patients with acute ischemic stroke. *Stroke* **2000**, *31*, 1863−1870.
(64) Kane, C. J. M.; Hebda, P. A.; Mansbridge, J. N.; Hanawalt, P. C. Direct evidence for spatial and temporal regulation of transforming growth factor β1 expression during cutaneous wound healing. *J. Cell. Physiol.* **1991**, *148*, 157−173.
(65) Wang, X.-J.; Han, G.; Owens, P.; Siddiqui, Y.; Li, A. G. Role of TGFβ-mediated inflammation in cutaneous wound healing. *J. Invest. Dermatol. Symp. Proc.* **2006**, *11*, 112−117.
(66) Wahl, S. M.; Hunt, D. A.; Wakefield, L. M.; McCartney-Francis, N.; Wahl, L. M.; Roberts, A. B.; Sporn, M. B. Transforming growth factor type beta induces monocyte chemotaxis and growth factor production. *Proc. Natl. Acad. Sci. U.S.A.* **1987**, *84*, 5788−5792.
(67) Tsunawaki, S.; Sporn, M.; Ding, A.; Nathan, C. Deactivation of macrophages by transforming growth factor-β. *Nature* **1988**, *334*, 260−262.
(68) Edwards, D. R.; Murphy, G.; Reynolds, J. J.; Whitham, S. E.; Docherty, A. J.; Angel, P.; Heath, J. K. Transforming growth factor β modulates the expression of collagenase and metalloproteinase inhibitor. *EMBO J.* **1987**, *6*, 1899−1904.
(69) Rousselle, P.; Braye, F.; Dayan, G. Re-epithelialization of adult skin wounds: Cellular mechanisms and therapeutic strategies. *Adv. Drug Deliv. Rev.* **2019**, *146*, 344−365.
(70) Badiavas, E. V.; Zhou, L.; Falanga, V. Growth inhibition of primary keratinocytes following transduction with a novel TGFβ-1 containing retrovirus. *J. Dermatol. Sci.* **2001**, *27*, 1−6.
(71) Jeong, H.-W.; Kim, I.-S. TGF-β1 enhances βig-h3-mediated keratinocyte cell migration through the $\alpha 3\beta 1$ integrin and PI3K. *J. Cell. Biochem.* **2004**, *92*, 770−780.
(72) Tredget, E. B.; Demare, J.; Chandran, G.; Tredget, E. E.; Yang, L.; Ghahary, A. Transforming growth factor-β and its effect on reepithelialization of partial-thickness ear wounds in transgenic mice. *Wound Rep. Regen.* **2005**, *13*, 61−67.
(73) Lu, L.; Saulis, A. S.; Liu, W. R.; Roy, N. K.; Chao, J. D.; Ledbetter, S.; Mustoe, T. A. The temporal effects of anti−TGF-β1, 2, and 3 monoclonal antibody on wound healing and hypertrophic scar formation. *J. Am. Coll. Surg.* **2005**, *201*, 391−397.
(74) Ashcroft, G. S.; Roberts, A. B. Loss of Smad3 modulates wound healing. *Cytokine Growth Factor Rev.* **2000**, *11*, 125−131.
(75) Galiano, R. D.; Michaels, J.; Dobryansky, M.; Levine, J. P.; Gurtner, G. C. Quantitative and reproducible murine model of excisional wound healing. *Wound Rep. Regen.* **2004**, *12*, 485−492.
(76) Hebda, P. A. Stimulatory effects of transforming growth factor-β and epidermal growth factor on epidermal cell outgrowth from porcine skin explant cultures. *J. Invest. Dermatol.* **1988**, *91*, 440−445.
(77) Hebda, P. A. The acceleration of epidermal wound healing in partial thickness burns by transforming growth factor-beta. *J. Invest. Dermatol.* **1989**, *92*, 442.
(78) Gailit, J.; Clark, R. A. F.; Welch, M. P. TGF-β1 stimulates expression of keratinocyte integrins during re-epithelialization of cutaneous wounds. *J. Invest. Dermatol.* **1994**, *103*, 221−227.
(79) Jenkins, C. L.; Vasbinder, M. M.; Miller, S. J.; Raines, R. T. Peptide bond isosteres: Ester or (*E*)-alkene in the backbone of the collagen triple helix. *Org. Lett.* **2005**, *7*, 2619−2622.
(80) Galiano, R. D.; Michaels, J.; Dobryansky, M.; Levine, J. P.; Gurtner, G. C. Quantitative and reproducible murine model of excisional wound healing. *Wound Rep. Regen.* **2004**, *12*, 485−492.
(81) Schroeder, A. B.; Dobson, E. T. A.; Rueden, C. T.; Tomancak, P.; Jug, F.; Eliceiri, K. W. The ImageJ ecosystem: Open-source software for image visualization, processing, and analysis. *Protein Sci.* **2021**, *30*, 234−249.

https://doi.org/10.1021/acschembio.1c00745
ACS Chem. Biol. 2022, 17, 314−321